Reaction Chemistry & Engineering

ROYAL SOCIETY OF CHEMISTRY

PAPER

View Article Online
View Journal | View Issue

Cite this: *React. Chem. Eng.*, 2026, **11**, 1228

Advances in continuous manufacturing of albuterol sulfate: optimization of an amination reaction in flow

Kimberly E. Penzer, Daniel G. Gregory, Samantha G. Kohn, Kaitlin E. Kay, Justin T. Turnage and James K. Ferri *

Albuterol sulfate, an asthma therapeutic, has historically been manufactured *via* batch processing yet is perennially listed on the FDA's drug shortage list. This work investigates the translation of a batch S_N2 amination reaction for synthesis of a key albuterol precursor towards continuous flow processing monitored with on-line ^{1}H NMR. The results detailed herein enable integration and scale-up of the unit operation within a larger end-to-end Advanced Manufacturing Technology (AMT) for continuous albuterol sulfate production. Initial batch screening studies were conducted to optimize process variables, determine kinetic parameters, and identify byproducts. Laminar and plug flow models were developed using batch kinetic data to simulate reactant conversion during molecular transit through a tubular reactor; the models were compared with experimental flow data at 20–60 °C. A pseudo first order flow model most accurately modeled the reaction in flow – enabling intelligent reactor design and scale-up by simulating yield at various temperatures (T), flowrates (Q), and residence times (τ). The experimental flow study demonstrated optimal solution yield (99.3 ± 4.6%) and conversion (99.0 ± 0.8%) of the starting material [50 mg ml^{-1}] when the reaction was performed in isopropanol at 60 °C with a 40 min τ. ^{1}H NMR was utilized as an on-line process analytical technology (PAT); key reaction species were identified and calibrated to enable quantification of concentration *via* an integrated flow cell. Ultimately, this work offers a continuous method of synthesizing a key API intermediate with on-line composition monitoring for integration and scale-up within a larger end-to-end AMT system to help alleviate drug shortages.

Received 20th October 2025,
Accepted 5th January 2026

DOI: 10.1039/d5re00465a

rsc.li/reaction-engineering

1. Introduction

In recent decades, the production of active pharmaceutical ingredients (APIs) has been gradually offshored from the United States to foreign nations with lower labor costs.[1] Rather than directly producing APIs domestically within the U.S., many pharmaceutical companies have prioritized supply chain management (SCM) and have opted to import APIs from abroad for drug formulation.[2] Today, the domestic production of APIs accounts for only 14% of the global API portfolio of small molecules.[3] In efforts to reverse this trend, recent policy initiatives[4] seek to reshore API manufacturing; the U.S. now has a stated goal to produce at least 25% of all APIs domestically by 2028.[5] A compelling strategy for achieving this goal is through the use of advanced manufacturing technologies (AMTs)[6,7] and continuous manufacturing (CM).[8] Here, we investigate the translation of a batch amination reaction for a key albuterol sulfate intermediate towards a streamlined, continuous flow reactor with on-line ^{1}H NMR. This automated flow system is currently being integrated within a larger end-to-end AMT for continuous manufacturing of albuterol sulfate (see Fig. 1).

APIs are well-known for their complexity in synthesis, are accompanied by strict regulatory standards, and are regarded as high value chemicals.[9] The development process from initial synthesis to regulatory approval of an API can span several decades, impacting the profitable lifespan of patents.[10,11] This implication has driven the pharmaceutical industry to predominantly utilize legacy batch processes, where regulations for product standards are deeply rooted.[12] During traditional pharmaceutical batch manufacturing, each process step is typically conducted within separate vessels with no direct flowing connection between reactors. This requires an iterative series of synthesis, material transfer, purification, and cleaning steps each achieved in unique vessels.[13]

Conversely, the continuous manufacturing of pharmaceuticals is a process in which chemical starting materials are transformed into APIs within interconnected

Department of Chemical and Life Science Engineering, Virginia Commonwealth University, 601 W Main St, Richmond, VA 23284, USA. E-mail: jkferri@vcu.edu

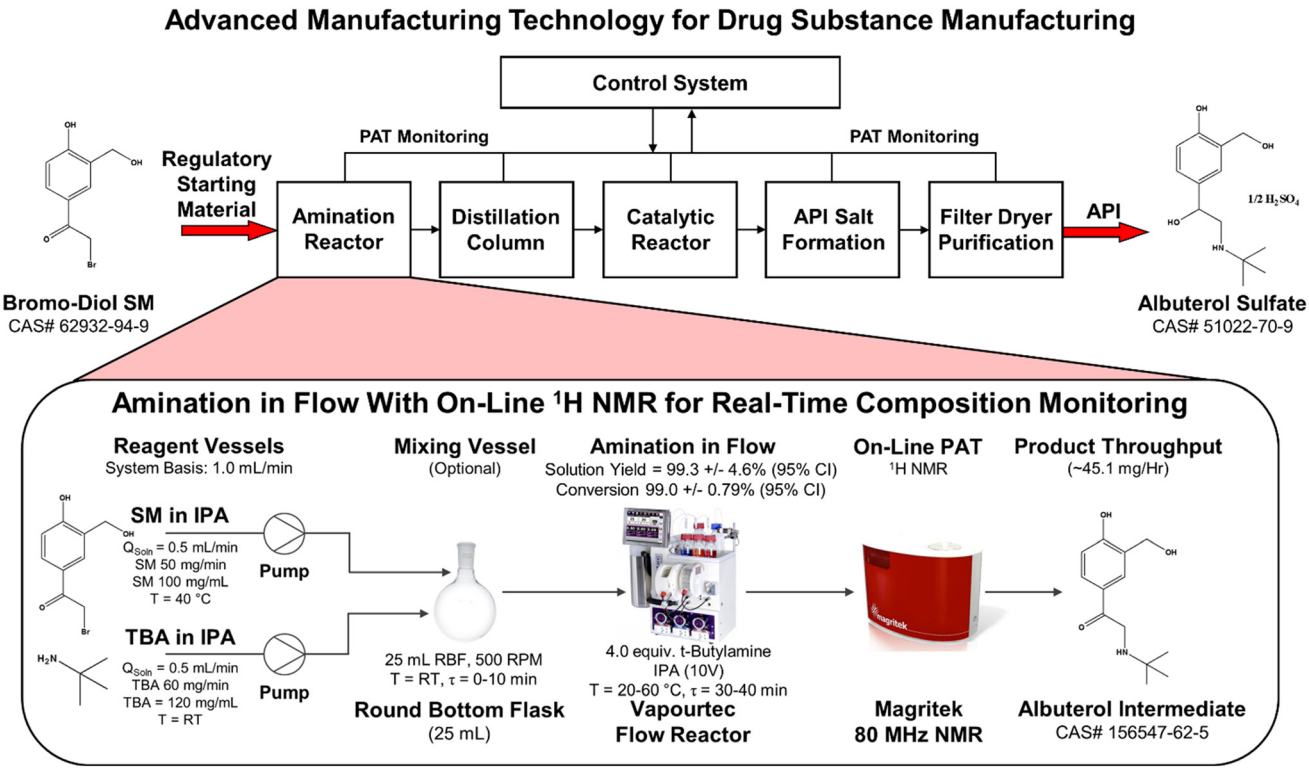

Fig. 1 A generalized schematic of the advanced manufacturing technology utilized for the continuous manufacturing of albuterol sulfate with highlighted focus on the continuous flow system used to perform the amination reaction in this work.

flow systems.[14] Until recently, the application of CM methods for the production of APIs has lacked research motivation; however, CM offers potential benefits including financial savings, centralized processing, a reduction in waste, and environmentally considerate chemistry.[15] Recent work has examined the use of amination reactions in flow for the CM of APIs.[16–20] Additionally, CM offers the ability to incorporate on-line process analytical technologies (PAT) within the system to enable real-time monitoring of composition.[21–23] Continuous manufacturing strategies have been shown to reduce the cost of production by up to 76%.[24]

In efforts to strengthen the U.S. pharmaceutical supply chain and modernize the industry, the Food and Drug Administration (FDA), biotech companies, and researchers are developing advanced manufacturing technologies,[7] such as modular, end-to-end continuous manufacturing systems.[25] This emerging vision entails a compartmentalized platform with interchangeable sub-modules which enable chemical transformations and key unit operations (*e.g.*, purification, formulation, and fill/finish packaging) for continuous API synthesis under current good manufacturing practices (cGMP).[8] Early CM success has been demonstrated through the Defense Advanced Research Project Agency's (DARPA) "Pharmacy on Demand" (PoD) program which resulted in a series of early CM systems.[26–30] These PoD systems have enabled the synthesis of multiple APIs, inspiring researchers to extend this technology to remediate the FDA's drug shortage list.[31] Here we highlight the development of a tubular amination reactor for integration within a larger CM system for the production of albuterol sulfate.

Albuterol sulfate (CAS# 51022-70-9) is a short-acting bronchodilator used to treat asthma patients.[32,33] However, there is currently a shortage of the nebulized albuterol sulfate solution (*i.e.*, drug product), as listed on the FDA's drug shortage list.[34,35] Albuterol has historically been produced through legacy batch processes involving a series of transformations with unstable intermediates,[36–39] and was first manufactured as an aerosol product in the 1960s by a U.K. manufacturer (*i.e.*, Allen and Hanburys).[40,41] The process chemistry was advanced and re-patented in 1988 by Esther Babad, *et al.* of Schering Corporation.[42,43] In the legacy process, an intermediate amination reaction and a catalytic hydrogenation reaction are key transformations necessary for the production of this lifesaving API.

This study highlights the development of a key transformation, an S_N2 amination reaction, for the production of an albuterol sulfate intermediate in flow. This reaction was optimized for performance in a tubular reactor with chemistry that produces improved yields compared to the traditional synthetic route. Several different synthetic routes were previously proposed by Babad; however, the highest amination yield was achieved when the reaction was performed in a batch reactor with IPA as the solvent medium and excess *t*-butylamine.[42] This

set of conditions achieved a 75% yield. Comparatively, the new process described in this study achieves +90% solution yields over a range of process conditions with reduced byproduct generation for continuous flow manufacturing with on-line ^{1}H NMR.

Scheme 1 presents the synthetic amination step investigated in this study. The reaction involves the conversion of a brominated starting material (molecule **1**, CAS# 62932-94-9) and *t*-butylamine (molecule **2**, TBA, CAS# 75-64-9) into a key aminated intermediate (molecule **3**, CAS# 156547-62-5) for downstream production of albuterol (see SI Scheme S2). The reaction was observed to form a dimerized impurity (molecule **4**) *via* a second parallel reaction. A series of batch reactions were first performed to screen the effect of process variables (*i.e.*, temperature, concentration, solvent) as well as to determine the kinetic parameters for development of a tubular flow reactor. Next, a tubular flow reactor was engineered to conduct the transformation. The tubular reactor reduced the amount of dimerized byproduct. Both laminar and plug flow models were constructed and compared against experimental flow results (see Fig. 1). Attention was then directed to incorporate proton nuclear magnetic resonance spectroscopy (^{1}H NMR) as an on-line process analytical technology (PAT), which has proven to be a successful reaction monitoring tool.[44] An analogous tubular flow system is currently being incorporated within a continuous GMP system with on-line ^{1}H NMR analysis. The resulting continuous amination process detailed herein can be readily scaled up within a larger end-to-end AMT system for the CM of albuterol sulfate.

2. Experimental

2.1. Materials

2-Bromo-1-[4-hydroxy-3-(hydroxymethyl) phenyl]ethan-1-one (Scheme 1 (**1**), 1 kg, purity >95%) was obtained from Ambeed and used as a precursor for the synthesis of **3** (Scheme 1). *Tert*-Butylamine (TBA) was purchased from Oakwood Chemicals (Scheme 1 (**2**), 500 g, purity >95%). Methanol was purchased from Fisher Chemical (4 L, HPLC grade, purity >99%); isopropanol was purchased from Fisher Chemical (20 L, ACS grade, purity >99%) and was dehydrated with molecular sieves from Fisher Chemical (grade 514, type 4A, 8–12 Mesh Beads).

2.2. Characterization methods

HPLC-MS analysis was performed using an Agilent 1200 Infinity Lab LC/MSD equipped with a Zorbax SB-C18 column (3.5 μm; 2.1 × 150 mm) to separate and identify primary species. UV diode array detectors (DAD) and a mass spectrometer (MS) provided absorbance and mass-to-charge ratio (*m*/*z*) data. HPLC-MS facilitated identification of key species (**1**, **3**, **4**) and impurities. HPLC-DAD was utilized to quantify species during reaction with an Eclipse XDB-C18 column (5.0 μm; 4.6 × 250 mm) and a gradient mobile phase (85% phosphoric acid buffer, 15% methanol) at 1.50 mL min^{-1}. Reaction samples were filtered, diluted in methanol (1–4 mg mL^{-1}), and stored at −24 °C prior to analysis. Calibration curves were constructed using commercial standards for **1**, an in-house synthesized 95% pure standard for **3**, and a response factor approximation for **4** based on chromophore counts of **1** and **3**. See SI for representative

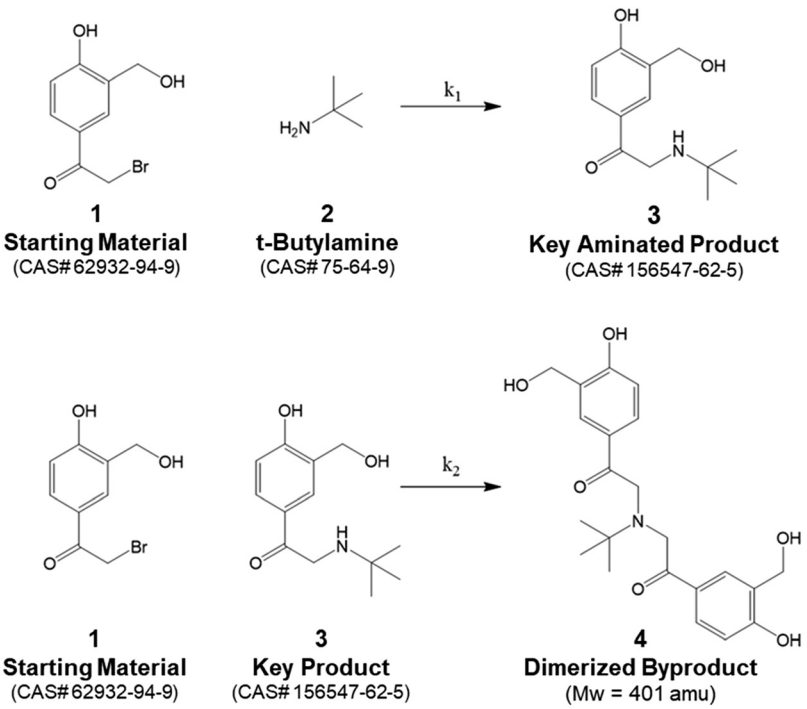

Scheme 1 Reaction schemes showing the conversion of **1** and **2** into **3** (k_1) as well as **1** and **3** into **4** (k_2).

data. Benchtop NMR was performed with a Magritek Spinsolve 80 MHz Carbon Ultra for on-line reaction analysis and complementary HPLC characterization. Mnova was utilized for data processing. Analysis modes included 1D1H, carbon satellite decoupling (*i.e.*, CDEC, $^{1}H\{^{13}C\}$), and solvent suppression (WET SUP). Calibration linearity was investigated for species **1**, **2**, and **3**. Samples were prepared *via* filtration without dilution.

2.3. Batch studies

Amination reactions (3 h) were conducted at 0–70 °C with reactant concentrations of 10–100 mg mL^{-1}. In a 100 mL round-bottom flask, **1** was dissolved in MeOH or dried IPA under nitrogen with magnetic stirring. Internal temperature was monitored, and a condenser was employed for reactions above 40 °C. Once the set point temperature was reached, four molar equivalents of TBA (**2**) were introduced *via* syringe pump. HPLC samples were collected at t = 0 and t = 3 h for conversion and yield analysis. Kinetic studies included batch reactions at 20, 40, and 60 °C in MeOH (40 mg mL^{-1} **1**) and IPA (25 mg mL^{-1} **1**), with **2** in 4 : 1 molar excess on a 50 mL scale. Aliquots were rapidly collected and analyzed *via* HPLC to monitor species evolution. An excess reagent study was conducted in IPA at 40 °C with excess molar equivalents consisting of 10, 15, and 20× *t*-butylamine, and with **1** at 100 mg mL^{-1} on a 50 mL scale. Calorimetry was performed using a Mettler Toledo EasyMax 102 Advanced reactor with a heat calibrator (HFCal) to quantify reaction enthalpy in MeOH and IPA. Reactions were conducted at 35 °C with **1** (100 mg mL^{-1}) on a 50 mL scale, and four equivalents of TBA were delivered *via* syringe pump. Temperature and heat flow data were logged. Heat capacity measurements were performed pre- and post-reaction. Final aliquots were analyzed *via* HPLC for quantification.

2.4. Flow studies

Flow studies were conducted in a Vapourtec E-series flow reactor with residence times (τ) of 3.67–60 min and tubing diameters of 1/16–1/8″. Dried IPA served as the reaction medium at temperatures ranging from 20–60 °C. A vessel contained **1** (100 mg mL^{-1}) at 40 °C, while a second vessel held **2** (120 mg mL^{-1}) at room temperature, ensuring a 4 : 1 molar ratio. During mixing, both a pure tubular reactor setup and a hybrid CSTR-tube flow setup were examined to assess radial mixing effects. Solutions of **1** and **2** were separately pumped and combined at a T-junction (tubular flow) or CSTR (optional hybrid setup). The optional CSTR utilized a 25 mL round bottom flask (RBF) to premix the components within the vessel while maintaining a 10 min residence time. The combined stream was then passed through 20–40 mL of coiled tubing which was enclosed within a glass container. The reactor was heated with flowing air while on-line temperature monitoring was recorded by the Vapourtec system. Outlet samples were filtered and analyzed *via* off-line HPLC and NMR. For on-line flow NMR studies, a manual valve was utilized to periodically divert flow to the NMR upon which a 30 second scan was performed in stop-flow mode; during this time, the primary process stream was directed into a product collection vessel. The flow setup is depicted in Fig. 1.

3. Results & discussion

3.1. Batch reaction performance

Initial batch screening reactions were conducted as described in section 2.3 to evaluate the effects of temperature, initial concentration of starting material (**1**), and solvent choice on production of the aminated product (**3**). Fig. 2 presents the impact of these variables on the conversion of species **1**, **3**, and **4** during batch screening studies. The amination reaction is susceptible to the formation of oligomeric byproduct species as detected *via* LC-MS (see Fig. S2). The primary impurity byproduct consisted of a dimerized species (**4**).

In Fig. 2A, non-dimensionalized concentration (θ) is plotted against temperature, normalizing selectivity and yield across each species. Here, θ is defined in eqn (1), where A is the area of the HPLC peak compared to the maximum and minimum concentration for species i under condition j. In MeOH, optimal conversion occurs between 20–40 °C. At 20 °C, selectivity towards species **3** is maximized, but complete conversion of the starting material, **1**, is not achieved. In IPA, optimal conversion is observed at 40–60 °C, with complete conversion of **1** at 40 °C; while the selectivity towards the dimer increases as the temperature is elevated above 40 °C. When below 40 °C, **1** remains largely insoluble in IPA [100 mg mL^{-1}] and limits the reaction.

$$\theta_i = \frac{A_{ij} - A_{i_{\min}}}{A_{i_{\max}} - A_{i_{\min}}} \quad (1)$$

Fig. 2B examines the effect of initial SM concentration, **1**, in both solvents. In MeOH, optimal performance occurs between 20–40 mg mL^{-1}. At 20 mg mL^{-1}, the formation of **3** is maximized, while selectivity towards the dimer impurity, **4**, is minimized; however, **1** was not fully converted under these dilute conditions. At 40 mg mL^{-1}, full conversion is achieved, but product yield decreases as the formation of the dimer increased. In IPA, the concentration of SM did not significantly impact the selectivity towards **3** and **4**; however, full conversion of SM was achieved at 100 mg mL^{-1}, making this the optimal condition. A table providing the solubility limits of **1** is provided in the SI (see Table S3).

Calorimetry experiments were performed to quantify the intrinsic molar enthalpy of reaction (ΔH_r) in MeOH and IPA following the procedure in section 2.2; Table 1 summarizes these results. The reaction was exothermic in both solvents; therefore, ΔH_r values are reported as the absolute magnitude of the enthalpy change ($|\Delta H_r|$) in kJ per mole of limiting reagent. The larger $|\Delta H_r|$ observed in MeOH corresponds to a greater effective heat release under process conditions and

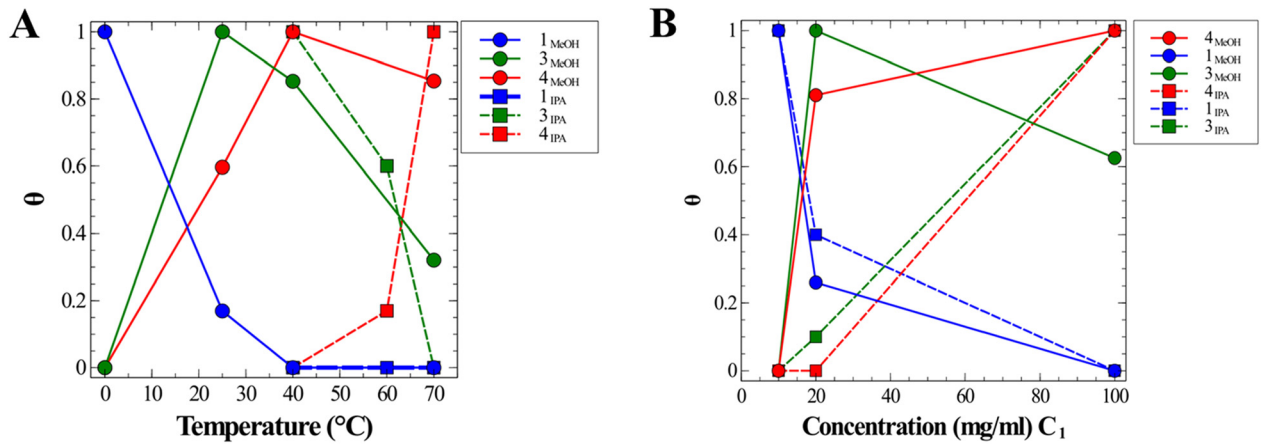

Fig. 2 Batch screening reactions, effect of (A) temperature and (B) concentration on product selectivity and yield *via* the non-dimensionalized concentration (θ) of components **1** (blue), **3** (green), and **4** (red). The reactions were run with four equivalents of **2**. Samples were measured after 3 hours of reaction time to observe the effects of temperature (A) and initial concentration of **1** on product selectivity and yield (B). Results for the reaction in IPA are plotted with dashed lines and for the reaction in MeOH with solid lines.

Table 1 Intrinsic molar enthalpy of reaction (ΔH_r) measured for the amination reaction in MeOH and IPA. 95% confidence interval values are listed

Solvent	ΔH_r (kJ mol^{-1})	95% CI
IPA	179.08	1.43
MeOH	265.74	5.05

necessitates additional thermal management during processing in MeOH.

Kinetic parameters were determined from the experimental batch data to inform reactor design for continuous operation in flow. Two approaches were employed for cross-validation including operation under standard concentrations at multiple temperatures (20–60 °C) and with excess reagent. Fig. 3 plots the concentration profiles of **1**, **3**, and **4** over time in MeOH (Fig. 3A) and IPA (Fig. 3B). As **1** is consumed, **3** and **4** form accordingly. MATLAB was utilized to solve the coupled ordinary differential equations (ODEs) which govern the batch reaction kinetics (see SI). The rate constants for product (k_1) and byproduct (k_2) formation were determined at multiple temperatures (Table 2), while Arrhenius analysis (see Fig. S4) was used to extract the activation energies (E_A) and Arrhenius constants (A).

The reaction progressed faster at higher temperatures (see Fig. 3). However, when comparing solvents, the primary reaction which forms species **3** proceeded consistently faster in IPA than in MeOH at all temperatures (Table 2). Additionally, the formation of byproduct (**4**) was notably slower in IPA. The activation energy for the formation of **3** was markedly lower when operating in IPA *versus* MeOH. Similarly, the activation energy for the formation of **4** was higher when utilizing IPA. This data demonstrates that the use of MeOH results in a slower reaction and favors increased byproduct formation as compared to IPA.

A secondary method employing excess TBA, **2**, was conducted for complementary kinetic validation (see section 2.2). The logarithm of **1** was plotted against time to determine observed rate constants. This data was then extrapolated against initial TBA, **2**, to derive the true rate constant (0.0801 M^{-1} min^{-1}) *versus* the apparent rate constant

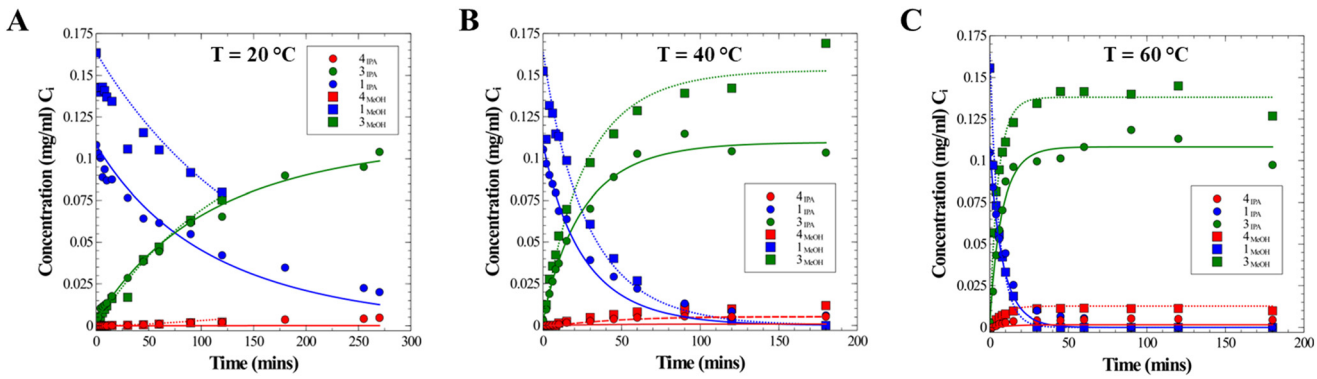

Fig. 3 The batch reaction conversion and product yields in MeOH (□, ----) and IPA (○, —) at (A) T = 20 °C, (B) 40 °C, and (C) 60 °C. The concentration of components **1** (blue), **3** (green), and **4** (red) are plotted against time. Points represent experimental values determined *via* HPLC whereas the curves are a fitted model. The reactions were run with four equivalents of **2**.

Table 2 Values for the kinetic rate constants (k_i), activation energy (E_A), and Arrhenius constant (A) for the reactions at 20–60 °C for both solvents (MeOH and IPA). The excess reagent method for k_1 in IPA at 40 °C is presented in parentheses

Parameter	Methanol		Isopropanol	
Temperature (°C)	k_1 (M^{-1} min^{-1})	k_2 (M^{-1} min^{-1})	k_1 (M^{-1} min^{-1})	k_2 (M^{-1} min^{-1})
20	0.0105	0.0032	0.0252	8.00×10^{-8}
40	0.0646	0.0043	0.1102 (0.0801)	2.51×10^{-6}
60	0.3098	0.1364	0.3557	0.0087
E_A (kJ mol^{-1})	68.79	74.56	53.77	233.14
A (M^{-1} min^{-1})	1.90×10^{10}	3.64×10^{10}	9.82×10^{7}	1.19×10^{34}

observed in excess TBA (0.1102 M^{-1} min^{-1}), as presented in Table 2. Ultimately, these results indicate the reaction follows second order kinetics when operating within a batch process, as commonly defined for S_N2 reactions.[45]

3.2. Flow studies

The effects of residence time and solvent selection were investigated in a tubular reactor under flow following the procedure listed in section 2.4. Fig. 4 plots the percent solution yield and conversion *versus* residence time for flow reactions at 40 °C. The reaction in IPA outperformed MeOH across all residence times by approximately 10% in both solution yield (Fig. 4A) and conversion (Fig. 4B). Conversion and solution yield increased and subsequently plateaued for both solvents as the residence time was extended. Due to its superior performance, IPA was selected for subsequent flow studies. Additionally, the flow reactor limited the production of oligomerized species in comparison to the batch amination reactions (see Table S3). This is likely a result of diffusive transport limitations which exist under laminar flow, which limit the ability of the SM to diffuse radially and form oligomerized species with the key aminated intermediate.

Next, experimental flow reactions were conducted to confirm operation in flow and to validate kinetic flow models using the methodology listed in section 2.4. The flow reactor was kinetically modeled in both laminar and plug flow, *i.e.*, with low and high respective Reynolds numbers (Re); see derivation in SI section 2–3.[46,47] Traditional plug flow kinetic models assume a turbulent, well mixed flow profile. However, alcohol-based solvents traveling at low flow rates are well within the laminar flow regime (*i.e.*, Re $<$ 2100). Thus, a laminar flow kinetic model was derived for both first (see eqn (2)) and second order kinetics (see eqn (3)) to model the reaction in flow. C_x denotes the concentration at position x, while the Damkohler number ($Da_n = kC_{A_0}^{n-1}\bar{t}$) provides a ratio of the rate of reaction to the residence time. Here x can be the concentration at either the exit or the inlet (*i.e.*, A_0) for species A (*i.e.*, the SM). Experimental concentrations, determined *via* HPLC, were plotted *versus* residence time for comparison with each model (Fig. 5).

A sensitivity analysis was conducted to assess the kinetic rate constants for each flow model. Fig. 5 presents conversion predictions for a laminar flow reactor (LFR, Fig. 5A) and a plug flow reactor (PFR, Fig. 5B) under first- and second-order kinetics (*i.e.*, for notation: LFR^{1st}, LFR^{2nd}, PFR^{1st}, PFR^{2nd} where superscripts denote reaction order). For a first-order reaction with k varying from 0.5–1.3 min^{-1}, the flow regime significantly affected conversion predictions at lower k values. In second-order kinetics, both reactor models followed similar trends. Across all conditions, model predictions were highly sensitive to k.

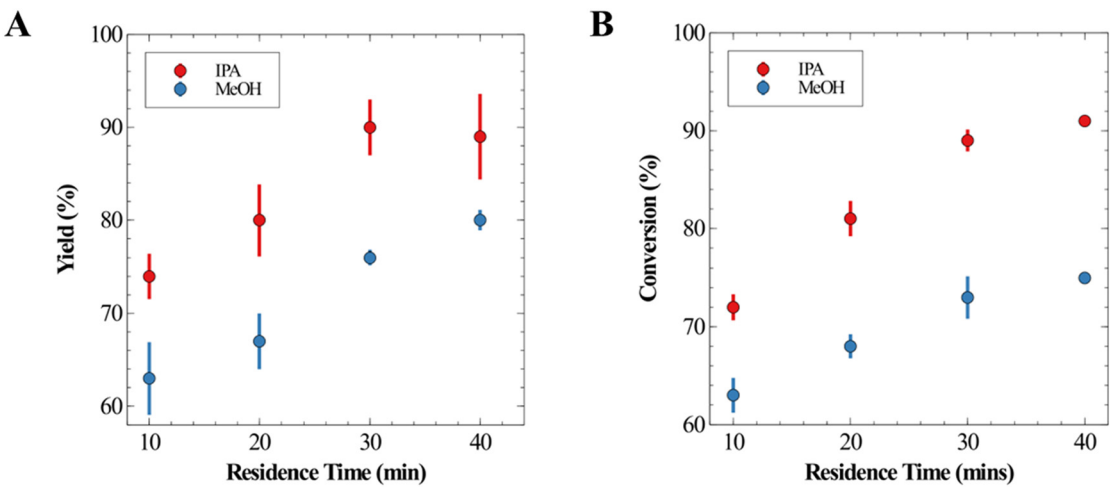

Fig. 4 Continuous flow amination, effect of residence time in IPA and MeOH on (A) solution yield and (B) conversion at 40 °C. Experimental results are represented by points (o) with error bars determined by a 95% confidence interval.

$$c_{\text{exit}} = C_{A_0}\left[\left(1-\frac{\text{Da}}{2}\right)\exp\left(\frac{-\text{Da}}{2}\right)+\frac{\text{Da}}{4}E_1\left(\frac{\text{Da}}{2}\right)\right] \quad (2)$$

$$c_{\text{exit}} = C_{A_0}\left[\frac{\text{Da}^2\log(-\text{Da})}{2}+\frac{\text{Da}^2\log(-\text{Da}-2)}{2}-\text{Da}+1\right] \quad (3)$$

A fit was applied to the experimental data by varying the rate constant until a curve of best fit was created. The values for the fitted kinetic parameters are shown in Table 3 with comparison to the batch kinetic parameters discussed previously. The fitted first-order PFR model had the smallest percentage difference (Δ = 32%) between the experimental results and fitted rate constant (*i.e.*, k = 0.34 min^{-1}). The flow rates employed at this scale ($Q \sim$ 1.0 mL min^{-1}) are conducive to laminar flow (*i.e.*, Re < 2100), however the sensitivity analysis between LFRs and PFRs of a first order reaction show similar conversion predictions (Fig. 5A and B). Thus, a pseudo-first-order reaction behavior likely exists when operating under flow with limited radial diffusion. Additionally, both higher order models (*i.e.*, LFR^{2nd} and PFR^{2nd}) present large discrepancies (*i.e.*, 141% difference) *versus* the batch kinetic parameters, further evidence confirming the flow reaction follows pseudo-first-order kinetics.

The differences in yield and conversion for the reaction as performed in a true tubular reactor *versus* a hybrid setup (*i.e.*, incorporation of a small CSTR mixing vessel prior to the tubular reactor) were observed to be statistically insignificant. Both configurations could accomplish 99% conversion of **1** at 60 °C with a residence time of 40 minutes in IPA.

3.3. ^{1}H NMR process analytical technology study

Proton NMR was utilized as an on-line PAT to analyze the evolving amination product and excess amine after exiting the tubular reactor for integration with the AMT system (see Fig. 6). To enable on-line PAT monitoring, the chemical species were first analyzed *via* traditional off-line NMR analysis within standard NMR tubes to identify the key proton signatures unique to each molecular species. Next, a series of calibration curves were created to accurately quantify chemical composition in flow. Finally,

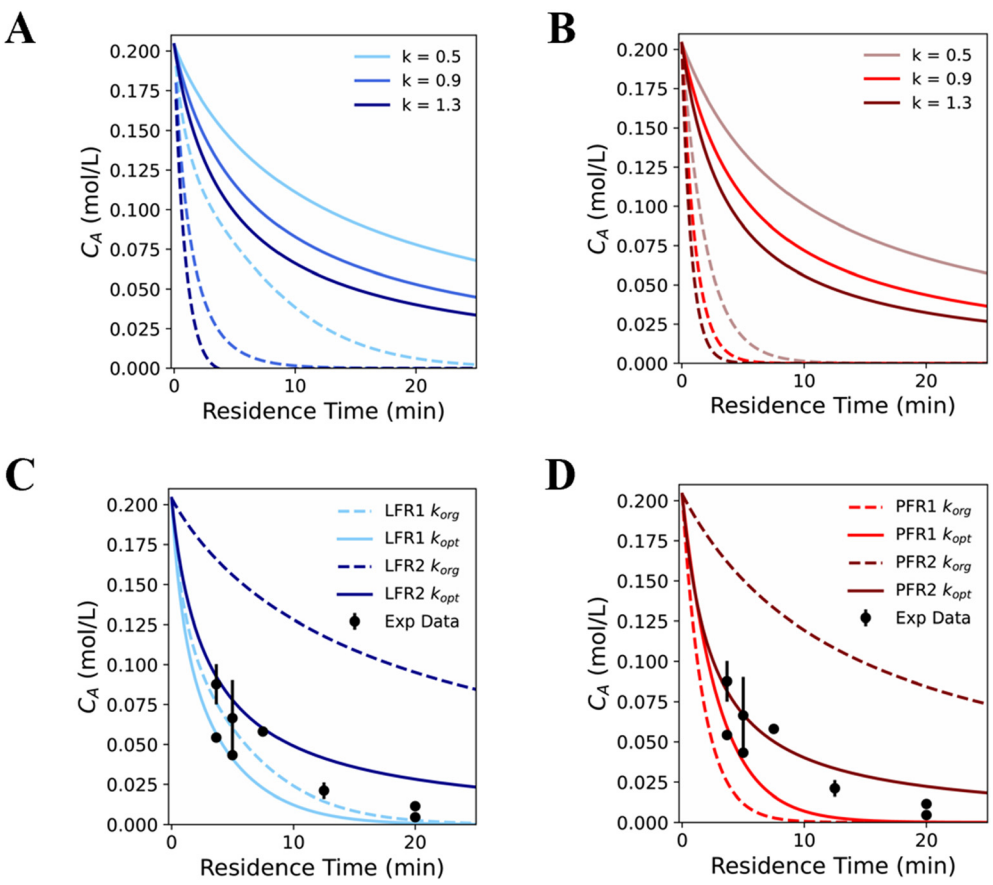

Fig. 5 Rate constant sensitivity analysis (k = 0.5–1.3) of developed flow models (LFR^{Order}, PFR^{Order}) for the conversion of **1** over time in isopropanol at 60 °C. (A): LFR^{1st} (dashed), LFR^{2nd} (solid), (B): PFR^{1st} (dashed), PFR^{2nd} (solid). Experimental and modeled concentration profiles for laminar flow (C) and plug flow (D) reactors at varying residence times. The Reynolds number (Re) varied from 6.4 to 69.7. Conversion models using the best-fit (solid curves) and original rate constants (dashed curves) are shown for first- and second-order reaction models, with error bars representing experimental uncertainties.

Table 3 Comparison of kinetic rate constants determined in batch experiments *versus* those determined by fitting flow models for LFR and PFR reactors. The percentage difference (%) between the kinetic rate constants

Flow model	k_{Batch} Experimental	k_{Flow} Simulated	%Difference (Δ)
LFR^{1st}	0.47	0.67	35%
LFR^{2nd}	0.35	2.00	141%
PFR^{1st}	0.47	0.34	32%
PFR^{2nd}	0.35	2.00	141%

the system was configured for on-line ^{1}H NMR flow analysis downstream from the LFR, as depicted in Fig. 1. During on-line analysis, the process stream was periodically diverted to the NMR using a manual valve to enable time-resolved characterization.

Fig. 6A and B presents representative off-line proton NMR spectra for species **1** and **3** with shaded regions highlighting key peaks including the aromatic protons (~10.5–11.5 ppm) and species-unique protons (*e.g.*, geminal protons at ~8.0 ppm). The inset provides simulated peak positions as predicted by ChemDraw, which match the relative peak positions of the experimental results (see Fig. S6). Solvent peaks were also observed in the spectra; however, these signals were suppressed *via* software (*i.e.*, Mnova, WET SUP mode) and are observed as downward oriented artifact peaks.

A series of NMR calibration curves were created for the SM and aminated product in IPA. This was accomplished using a glass flow cell which was inserted into the NMR and charged using a peristaltic pump. A five-point calibration curve was created for standard one-dimensional analysis (1D1H), carbon satellite decoupling (CDEC), and with solvent suppression modes to which a 95% confidence interval was determined for each calibration. The calibration curves provided a linear range at concentrations ranging from ~1–120 mg mL^{-1} when utilizing solvent suppression and satellite decoupling (*i.e.*, ^{1}H{^{13}C}). The precision and linearity of the calibration curve changed insignificantly depending on the processing mode. The deviation in slope only decreased from 2.7% to 2.4% for component **1** and 0.02% to 0.46% for component **3** when comparing 1D1H to solvent suppression.

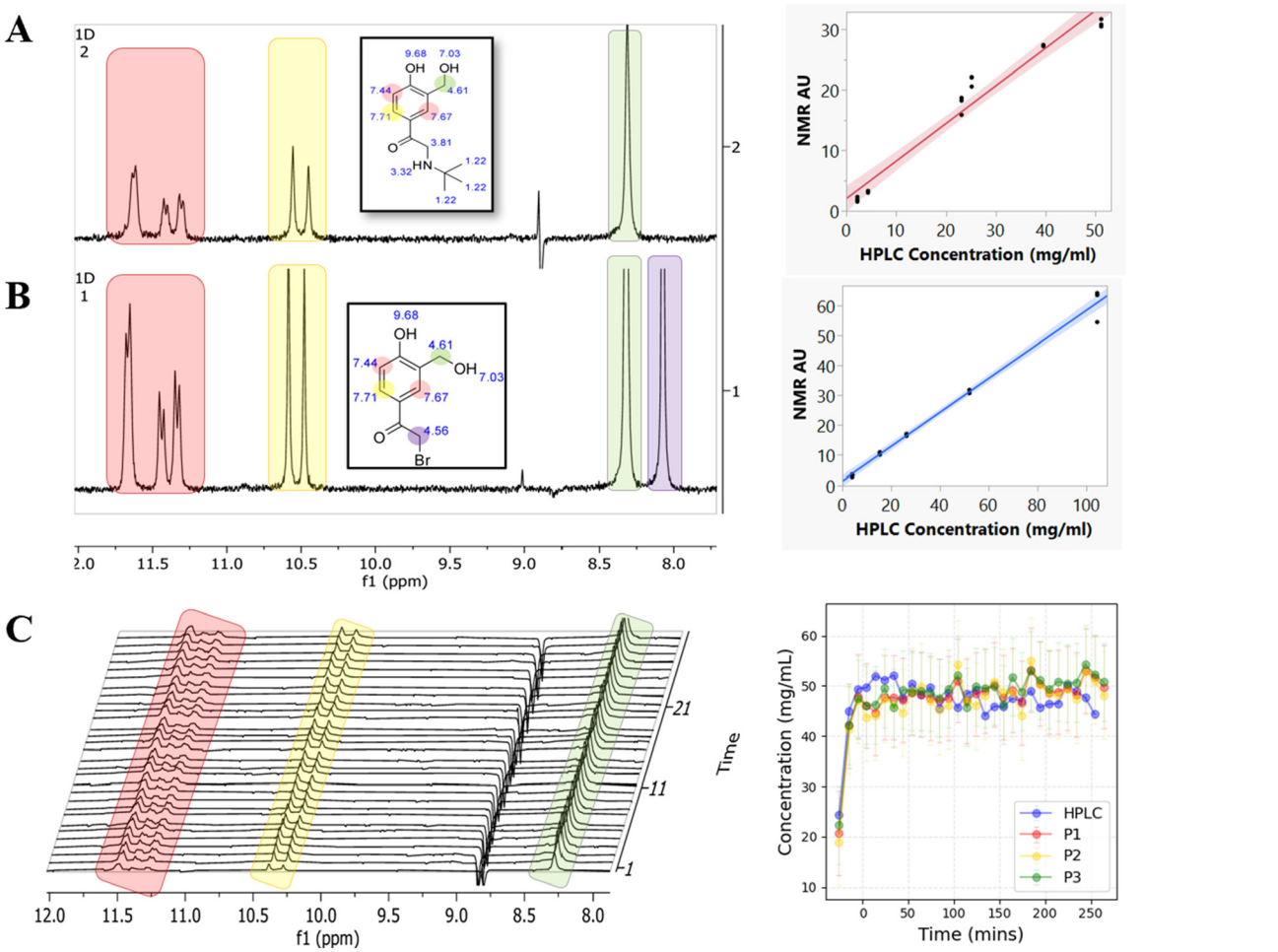

Fig. 6 Proton NMR spectra for (A) the aminated product and (B) the starting material with peak labeling simulated *via* ChemDraw (center inset) and calibration curves (right inset); (C) on-line ^{1}H NMR flow data with orthogonal comparison with off-line HPLC (inset). The ^{1}H NMR spectra were collected utilizing solvent suppression and satellite decoupling (^{1}H{^{13}C}).

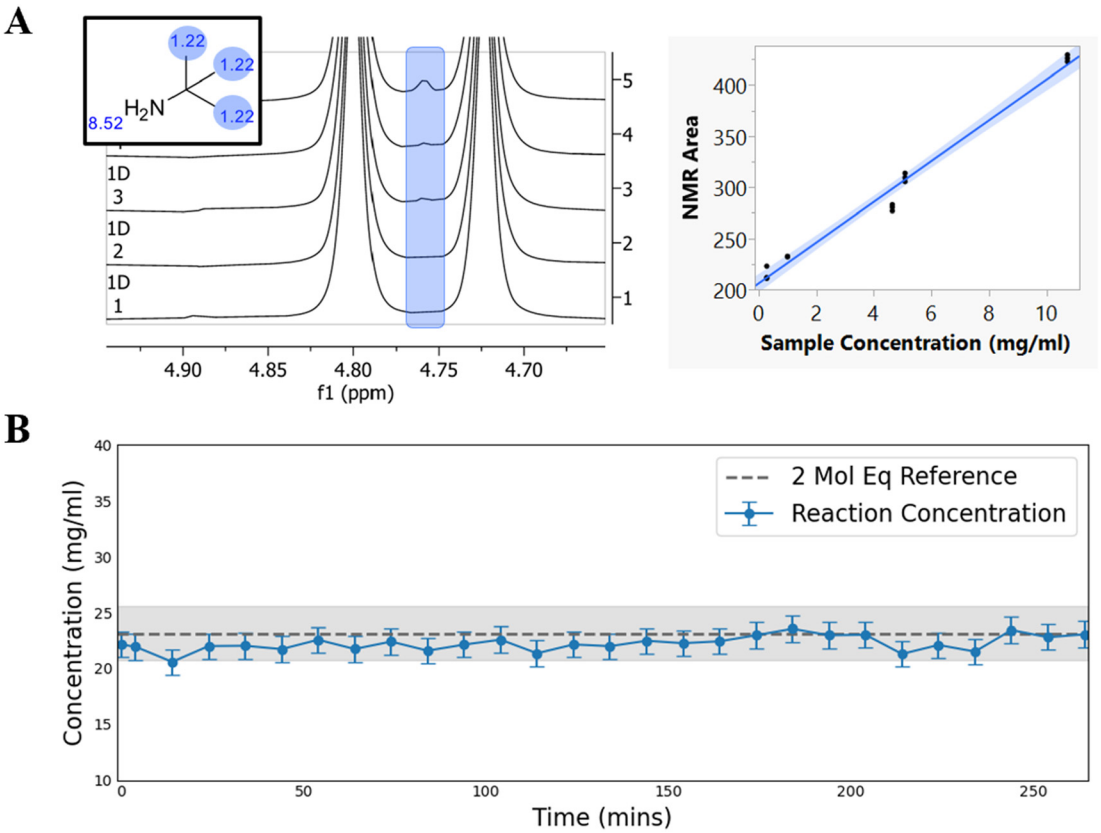

Fig. 7 (A) Proton NMR spectra for the amination reactant, species **2**, with peak labeling simulated *via* ChemDraw (top left inset) and calibration curves (top right inset); (B) on-line ^{1}H NMR flow data with orthogonal comparison to the theoretical reaction conversion. The ^{1}H NMR spectra were collected utilizing a standard 1D1H scan.

This 80 MHz ^{1}H NMR flow cell system enabled a lower limit of detection (LOD) of ~1.0 mg mL^{-1} when using the settings specified in section 2.2.

Fig. 7A presents representative off-line proton NMR spectra for species **2** with shaded regions highlighting key protons (~4.77 ppm). The inset provides simulated peak positions as predicted by ChemDraw (see Fig. S6). A series of NMR calibration curves were also created for species **2** in IPA. Similarly, for the before-mentioned species **1** and **3**, calibration was accomplished using a glass flow cell which was inserted into the NMR and charged using a peristaltic pump. A calibration curve was created for standard one-dimensional analysis (1D1H) to which a 95% confidence interval was determined. The calibration curve provided a linear range at concentrations ranging from ~1.0–10 mg mL^{-1} when utilizing a standard one-dimensional analysis (1D1H).

After developing calibration curves for each major component, the NMR system was configured as an on-line PAT to both identify and quantify species within the process stream after exiting the flow reactor (see Fig. 6C and 7B). Next, chemical composition was orthogonally analyzed with off-line HPLC to statistically validate ^{1}H NMR as an on-line PAT (see Fig. 6C, Inset). Chemical composition of species **2** was analyzed against the theoretical amount expected to be remaining based upon stoichiometric conversion with species **1** (see Fig. 7B). ^{1}H NMR provided a powerful on-line PAT for analysis of chemical components **1**, **2** and **3**, in flow and closely matched the off-line analytical results as quantified *via* complementary HPLC (see Fig. 6C, Inset).

3.4. Process overview and AMT integration

The industrial production of albuterol sulfate has historically been conducted in batch operations *via* key process transformations including amination, catalytic hydrogenation, and API salt formation.[32,33,36–43,48] In each documented process, an amination reaction plays a central role in the synthesis of an intermediate precursor to albuterol. This study examined optimization of the process chemistry and reactor engineering necessary to manufacture a key aminated intermediate species for downstream production of albuterol sulfate in flow (see SI Scheme S2). Ultimately, this unit operation and its associated kinetic models enable integration within a larger end-to-end AMT platform (see Fig. 1).[49]

First, a series of batch screening studies were conducted to validate the new process chemistry, obtain preliminary process parameters, identify impurity byproducts, and quantify kinetic and thermodynamic parameters. A bromo-diol starting material (**1**) was utilized for this reaction with

four excess molar equivalents of *t*-butylamine (**2**) to form the aminated albuterol precursor (**3**). This reaction was conducted at moderate temperatures (T = 0–60 °C) and in common, low-cost alcohol solvents (*i.e.*, MeOH and IPA). The reaction was exothermic in both MeOH and IPA, with a ΔH_r of 265.74 and 179.08 kJ mol^{-1} respectively. Batch kinetic modeling enabled determination of key kinetic parameters (*e.g.*, k_i, E_a, A) for process translation. This kinetic study demonstrated that the reaction followed second order kinetics for both MeOH and IPA (see Table 2), a trend commonly reported for batch S_N2 reactions in literature.[43,47]

Next, the batch process chemistry was translated into a continuous operation in flow to enable S_N2 amination and incorporation within the AMT system. In both batch and flow studies, four equivalents of TBA were found to successfully promote S_N2 amination to enable full conversion of the SM and +90% solution yield of the product (**3**). Additionally, small amounts of oligomeric species (*i.e.*, dimerized SM species) were produced in a parallel side reaction as identified with LC-MS (see Fig. S1–S2). Optimal flow conditions were observed within the tubular reactor at 60 °C in IPA with a 40-minute residence time and an initial SM concentration of 50 mg mL^{-1}; this enabled a 99.3 ± 4.6% solution yield of **3** and a 99.0 ± 0.8% conversion of **1** in flow (see Fig. 4). The process detailed herein can achieve a 76.8% isolated yield after purification *via* Büchner funnel filtration and recrystallization. This process exceeds the ~75% isolated yields for comparable amination steps in traditional batch studies for the production of albuterol.[36,38,42]

The tubular flow reactor was modeled as both a laminar and plug flow reactor for comparison with experimental results. Traditional PFR's operate with high Reynolds numbers (*i.e.*, Re > 4000) and can be assumed well mixed in when in the turbulent flow regime. Conversely, LFR's operate in the laminar flow regime with low Reynolds numbers (*i.e.*, Re < 2100) and maintain standing streamlines.[50] Consequently, LFR's undergo limited radial mixing which can reduce the apparent kinetics of the reaction as chemical species must diffuse radially in order to react, as was noted by a reduction in the dimerized material. In our process, which operates at low flowrates in IPA (Q ~ 1.0 mL min^{-1}) the system is well within the laminar regime (Re < 100) with minimal difference between experimental and simulated results. Similarly, the system possesses moderate-to-high Péclet numbers (Pe), which is the effective ratio of advective transport to diffusion.[51] Thus, pseudo-first-order models most accurately modeled both the kinetics and inherent transport effects associated with the tubular amination reactor (see eqn (2), where k = 0.67 min^{-1} for a pseudo 1st order LFR and 0.34 min^{-1} for a pseudo 1st order PFR). A recent review by Taylor *et al.* supports these findings; Taylor notes that LFR and PFR models both accurately model flow reactions on this scale (*i.e.*, micro- to meso- flow scale) with minimal statistical variation between each model.[52]

Second order PFR and LFR kinetic models were considered, yet these models did not match flow data as well as the first order models. After reviewing the literature, limited model development was found for second-order reactions occurring in laminar flow, as the resulting research literature primarily focuses on reactions with equimolar amounts of reactants. This makes direct model comparison between our system and other studies difficult, but still offers meaningful insights related to reaction kinetics. In a study by Kien T. Nguyen *et al.*, the effects of flow regime were investigated on the kinetics of an equimolar second-order reaction occurring within a channel using a Lagrangian method.[53] Nguyen calculated the overall conversion, residence time, effective reaction rate coefficient, and reactor length necessary to achieve 80% conversion. Specifically, Nguyen modeled the effect of Pe number and demonstrated that systems with high Péclet numbers (Pe ≫ 1) can drastically reduce the apparent kinetics of a second order reaction in laminar flow. This finding generally aligns with our study as presented in Fig. 5A and B and demonstrates the sensitivity of apparent kinetic parameters to Pe.

The use of four excess molar equivalents of TBA facilitate multiple roles including (I) the first TBA equivalent nucleophilically reacts with the alkyl halide to produce the aminated product, (II) the second amine equivalent acts as a weak base to scavenge the newly released HBr species while forming a TBA·HBr salt, and (III) the final two free-amine equivalents help drive the reaction to completion. Primary amines (*i.e.*, 1°) such as TBA act as strong nucleophiles due to the presence of a lone pair electron group which rapidly reacts with alkyl halides *via* an S_N2 reaction.[54] However, 1° amines are also susceptible to continued side reactions which produce higher order amine oligomers (*e.g.*, secondary, 2°, tertiary, 3°, and quaternary ammonium salts).[55] This was observed through the formation of a dimerized species which constituted the primary reaction impurity. The dimer contains ~2× chromophores in comparison to **1** and **3**; thus, its concentration was calculated from the HPLC-DAD data *via* response factor scaling (see Fig. S3). The dimerized species was observed to be limited in concentration (*i.e.*, <1.0%) within the final process stream.

Additionally, the tubular flow reactor was observed to greatly reduce the generation of dimerized and oligomerized species as compared to reactions taking place within a batch CSTR-style system (see Fig. S7). This is likely a result of diffusive transport limitations which exist during laminar flow within the tubular reactor. As the process stream travels along the axial dimension of a tubular reactor, limited radial diffusion will occur due to the presence of standing laminar streamlines. These transport limitations ultimately reduce the ability of the SM and intermediate from mixing radially and will prevent the formation of oligomeric species. Conversely, when the reaction is conducted within a well-mixed CSTR, intimate mixing is enabled which leads to a promotion of oligomerized species (see Table S4).

Another variable taken into consideration in this work was the choice of solvent medium (*i.e.*, MeOH *versus* IPA). Recent studies have examined the influence of solvent selection on

product distribution and its effect on the relative and absolute rate constant of a reaction.[56] The reaction screening experiments (see Table 2) showed that even at lower concentrations of SM (**1**), the kinetics were faster in IPA than in MeOH. In a related literature study, it was found that the most prominent solvent property which impacts the kinetics of a reaction is solvent polarity.[57] For transformations which form molecules of ionic character, an increase in reaction rate can be observed with an increase in polarity. Conversely, for reactions forming molecules of non-ionic character, such as in our process, reaction rates decrease with an increase in solvent polarity. Thus, the reaction proceeds with faster kinetics in IPA, as it is a less polar solvent in comparison to MeOH, and offers a preferred environmental medium for synthesis. Similarly, the formation of dimerized salt species was substantially slower in IPA due to the effects of polarity. These trends are supported by comparing the solubility of albuterol sulfate in each solvent (see Table S2).

Investigations were then conducted to incorporate an on-line process analytical technology to quantify the aminated product for communication with the AMT controller. For reaction monitoring within a continuous system, on-line PAT's offer real-time feedback that can quantify product composition, ensure purity, and minimize waste. Specifically, on-line ^{1}H NMR was utilized in this study to quantify the amount of aminated product produced by the tubular reactor and to quantify the presence of excess TBA impurities. NMR offers a powerful on-line PAT tool due to its ability to provide real-time, non-invasive monitoring of chemical reactions and is rapidly becoming more popular in the process analytical technology space.[23,44,58,59] Additionally, NMR offers detailed insights into reaction kinetics, chemical structure, impurity identification, and product formation to enable precise control and optimization of a process. These characteristics make NMR an invaluable asset in both research and industrial applications for enhancing efficiency and ensuring product quality.

Alternative on-line PAT's including HPLC, UV-vis, FTIR, and Raman spectroscopy were considered; however, they did not offer the advanced capabilities of NMR. Both UV-vis and FTIR do not produce the required structural detail necessary to identify key molecular features within solution. Additionally, UV-vis and HPLC systems which utilize DAD's are unable to accurately detect impurity molecules which lack chromophores (*e.g.*, *t*-butylamine). Raman spectroscopy was found unsuitable for on-line analysis as the process solution was prone to strong fluorescence. Lastly, while HPLC is the standard for off-line analysis, the long acquisition time associated with this method introduces a significant time delay making it undesirable for on-line use.

In contrast, NMR enables real-time monitoring with data acquisition on the scale of seconds, making it a promising PAT tool for molecular characterization. Thus, ^{1}H NMR was utilized to validate chemical products in flow and to assess its on-line incorporation within a CM system. The analytical NMR results were observed to match complementary off-line HPLC analysis of the product stream with statistical certainty for the aminated product (**3**) while offering detection of t-butylamine (**2**), a key excess reagent. On-line ^{1}H NMR enabled quantification of these chemical species within the 1–120 mg mL^{-1} range, with a LOD ~1.0 mg mL^{-1}.

The resulting continuous amination flow system detailed herein constitutes a key unit operation which is currently being integrated within a continuous end-to-end manufacturing system for cGMP production of albuterol sulfate.[61] The continuous manufacturing system currently under development has demonstrated an overall isolated yield of 60.6%.[49] The final CM system will enable the purification of albuterol sulfate *via* recrystallization within an automated filter dryer. The resulting API will then be diluted, mixed with excipients, and packaged within injectable liquid vials as a packaged drug product. The use of on-line ^{1}H NMR as a PAT will validate the removal of the excess TBA and the dimerized byproduct to meet the International Conference on Harmonization's standards for drug substance purity and eliminate drug shortages.[25,60]

4. Conclusions

We detail the development of a continuous flow reactor system enabling S_N2 amination of a key albuterol sulfate precursor for integration within a continuous AMT manufacturing system for the production of albuterol sulfate. Process variables, such as temperature, initial concentration of starting material, and solvent medium, were screened in batch studies for their effects on conversion and selectivity. It was found that the temperature and solvent medium played a crucial role in the reaction kinetics. As reaction temperature was increased, the reaction progressed more rapidly; however, the selectivity towards a dimerized byproduct increased slightly in both solvent mediums. The reaction excelled in IPA *versus* MeOH, and enabled greater yields, higher conversions, and faster reaction rates under all experimental conditions. Additionally, the use of a tubular flow reactor reduced the formation of oligomeric byproducts. Optimal flow conditions were achieved at 60 °C in IPA with a 40-minute residence time and an initial concentration of 50 mg mL^{-1} of SM; this enabled a 99.3 ± 4.6% solution yield of **3** and 99.0 ± 0.8% conversion of **1** in flow.

A series of kinetic models were developed and compared against experimental data to simulate the conversion of starting material within a tubular flow reactor under various flow regimes. A pseudo-first-order kinetic model most accurately modeled the experimental results in flow. All investigated flow rates were well within the laminar flow regime. On-line ^{1}H NMR was integrated downstream from the reactor to quantify both chemical products and residual amine with a ~1.0 mg mL^{-1} limit of detection. The data provided by ^{1}H NMR statistically matched orthogonal off-line HPLC data. The resulting flow system constitutes a key unit operation for integration within a larger AMT system and can be scaled-up for continuous manufacturing of albuterol sulfate.

Author contributions

Author contributions are as follows: conceptualization, J.K.F., D.G.G., K.E.P.; methodology, J.K.F., K.E.P., D.G.G.; investigation, K.E.P., D.G.G., K.E.K., J.T.T., S.G.K.; writing—original draft, K.E.K., D.G.G.; writing–review & editing, K.E.P., D.G.G., J.K.F.; funding acquisition & resources, J.K.F.; supervision, J.K.F., D.G.G. The manuscript was prepared through the contributions of all authors. All authors have given approval to the final version of the manuscript.

Conflicts of interest

There are no conflicts to declare.

Abbreviations

ΔH_r	Heat of reaction
1D1H	One dimensional proton NMR spectroscopy
^{1}H NMR	Proton nuclear magnetic resonance
$^1H\{^{13}C\}$	Carbon satellite decoupling
AMT	Advanced manufacturing technology
API	Active pharmaceutical ingredient
CAS#	Chemical abstract services number
CDEC	Carbon satellite decoupling
cGMP	Current good manufacturing practices
CI	Confidence interval
CM	Continuous manufacturing
CSTR	Continuously stirred tank reactor
DAD	Diode array detector
DARPA	Defense Advanced Research Projects Agency
FDA	U.S. Food and Drug Administration
FTIR	Fourier transform infrared spectroscopy
GC	Gas chromatography
HPLC	High-performance liquid chromatography
ICH	International Council for Harmonization
IPA	Isopropyl alcohol
LFR	Laminar flow reactor
LOD	Limit of detection
MeOH	Methanol
MS	Mass spectrometry
NMR	Nuclear magnetic resonance
ODE	Ordinary differential equation
PAT	Process analytical technology
Pe	Péclet number
PFD	Process flow diagram
PFR	Plug flow reactor
PI	Process intensification
PoD	Pharmacy on demand
RBF	Round bottom flask
Re	Reynolds number
SCM	Supply chain management
SI	Supplementary information
SM	Starting material
TBA	*t*-Butylamine
UV-Vis	Ultraviolet-visible spectroscopy
WET SUP	Solvent suppression

Data availability

Additional data for this article is included in the supplementary information (SI): the SI includes process chemistry schemes, representative HPLC and LC-MS chromatograms, impurity profiles, solubility limits, chromophore analysis, and calorimetry data. Additionally, the kinetic rate laws are provided in the SI along with Arrhenius plots and derivation of first and second order laminar flow models. Supplementary information is available. See DOI: https://doi.org/10.1039/d5re00465a.

Acknowledgements

We are grateful to the U.S. Food & Drug Administration (FDA) for providing funds for this research through an award to the National Institute for Pharmaceutical Technology & Education (NIPTE) titled "A Model-Based Systems Engineering Approach to End-to-End Pharmaceutical Manufacturing of Liquid Dosage Forms" contract # BAA 75F40122C00122. We are grateful for additional funding provided by the Defense Advanced Research Projects Agency (DARPA) for the project titled: "Mobile System for GMP Manufacturing of Injectable and Inhalable Products" (DARPA-PS-24-12). The authors would also like to thank: Brandyn Kimball and Nabil Mouhajir for assistance on the project; Dr. Yingru Zhang of Lotus Separations in Princeton N. J. for assistance with HPLC method development; Ryan Blough and Dr. Anh Le-McClaine of Magritek for assistance with ^{1}H NMR data processing.

References

1 R. Ciriminna, C. Della Pina, R. Luque and M. Pagliaro, Reshoring Fine Chemical and Pharmaceutical Productions, *Org. Process Res. Dev.*, 2024, **28**, 3026–3034, DOI: 10.1021/acs.oprd.4c00219.
2 R. Ciriminna, C. Della Pina, R. Luque and M. Pagliaro, The Fine Chemical Industry, 2000–2024, *Org. Process Res. Dev.*, 2025, **29**, 1191–1196, DOI: 10.1021/acs.oprd.5c00010.
3 M. P. Socal, K. Ahn, J. A. Greene and G. F. Anderson, Competition And Vulnerabilities In The Global Supply Chain For US Generic Active Pharmaceutical Ingredients, *Health Aff.*, 2023, **42**, 407–415, DOI: 10.1377/hlthaff.2022.01120.
4 *Policy Considerations to Prevent Drug Shortages and Mitigate Supply Chain Vulnerabilities in the United States*, US Department of Health and Human Services, 2024.
5 *The White House Office of Science and Technology Policy, Bold Goals for Harnessing Research and Development to Further Societal Goals*, 2023.
6 A. Nelson and K. Koizumi, *National Strategy for Advanced Manufacturing*, National Science and Technology Council, 2022.
7 FDA and CDER, *Advanced Manufacturing Technologies Designation Program Guidance for Industry*, 2024.
8 A. Hyer, D. Gregory, K. Kay, Q. Le, J. Turnage, F. Gupton and J. K. Ferri, Continuous Manufacturing of Active Pharmaceutical Ingredients: Current Trends and Perspectives, *Adv. Synth. Catal.*, 2024, **366**, 357–389, DOI: 10.1002/adsc.202301137.

9 P. Pollak and R. Vouillamoz, in *Ullmann's Encyclopedia of Industrial Chemistry*, Wiley-VCH Verlag GmbH & Co. KGaA, Weinheim, Germany, 2013.
10 N. Shah, Pharmaceutical Supply Chains: Key Issues and Strategies for Optimisation, *Comput. Chem. Eng.*, 2004, **28**, 929–941, DOI: 10.1016/j.compchemeng.2003.09.022.
11 M. S. Lipsky and L. K. Sharp, From Idea to Market: The Drug Approval Process, *J. Am. Board Fam. Med.*, 2001, **14**, 362–367.
12 R. K. Singh, R. Kumar and P. Kumar, Strategic Issues in Pharmaceutical Supply Chains: A Review, *International Journal of Pharmaceutical and Healthcare Marketing*, 2016, **10**, 234–257, DOI: 10.1108/IJPHM-10-2015-0050.
13 R. Porta, M. Benaglia and A. Puglisi, Flow Chemistry: Recent Developments in the Synthesis of Pharmaceutical Products, *Org. Process Res. Dev.*, 2016, **20**, 2–25, DOI: 10.1021/acs.oprd.5b00325.
14 M. B. Plutschack, B. Pieber, K. Gilmore and P. H. Seeberger, The Hitchhiker's Guide to Flow Chemistry, *Chem. Rev.*, 2017, **117**, 11796–11893, DOI: 10.1021/acs.chemrev.7b00183.
15 J. S. Srai, C. Badman, M. Krumme, M. Futran and C. Johnston, Future Supply Chains Enabled by Continuous Processing-Opportunities and Challenges, *J. Pharm. Sci.*, 2015, **104**, 840–849, DOI: 10.1002/jps.24343.
16 C. Xue, J. Li, J. P. Lee, P. Zhang and J. Wu, Continuous Amination of Aryl/Heteroaryl Halides Using Aqueous Ammonia in a Teflon AF-2400 Tube-in-Tube Micro-Flow Reactor, *React. Chem. Eng.*, 2019, **4**, 346–350, DOI: 10.1039/c8re00216a.
17 P. Yaseneva, P. Hodgson, J. Zakrzewski, S. Falß, R. E. Meadows and A. A. Lapkin, Continuous Flow Buchwald-Hartwig Amination of a Pharmaceutical Intermediate, *React. Chem. Eng.*, 2016, **1**, 229–238, DOI: 10.1039/c5re00048c.
18 S. Falß, G. Tomaiuolo, A. Perazzo, P. Hodgson, P. Yaseneva, J. Zakrzewski, S. Guido, A. Lapkin, R. Woodward and R. E. Meadows, Continuous Process for Buchwald-Hartwig Amination at Micro-, Lab-, and Mesoscale Using a Novel Reactor Concept, *Org. Process Res. Dev.*, 2016, **20**, 558–567, DOI: 10.1021/acs.oprd.5b00350.
19 Z. Fülöp, P. Szemesi, P. Bana, J. Éles and I. Greiner, Evolution of flow-oriented design strategies in the continuous preparation of pharmaceuticals, *React. Chem. Eng.*, 2020, **5**, 1527–1555, DOI: 10.1039/d0re00273a.
20 V. R. L. J. Bloemendal, M. A. C. H. Janssen, J. C. M. Van Hest and F. P. J. T. Rutjes, Continuous one-flow multi-step synthesis of active pharmaceutical ingredients, *React. Chem. Eng.*, 2020, **5**, 1186–1197, DOI: 10.1039/d0re00087f.
21 C. Claaßen, K. Mack and D. Rother, Benchtop NMR for Online Reaction Monitoring of the Biocatalytic Synthesis of Aromatic Amino Alcohols, *ChemCatChem*, 2020, **12**, 1190–1199, DOI: 10.1002/cctc.201901910.
22 T. Maschmeyer, L. P. E. Yunker and J. E. Hein, Quantitative and Convenient Real-Time Reaction Monitoring Using Stopped-Flow Benchtop NMR, *React. Chem. Eng.*, 2022, **7**, 1061–1072, DOI: 10.1039/d2re00048b.
23 A. Friebel, E. Von Harbou, K. Münnemann and H. Hasse, Reaction Monitoring by Benchtop NMR Spectroscopy Using a Novel Stationary Flow Reactor Setup, *Ind. Eng. Chem. Res.*, 2019, **58**, 18125–18133, DOI: 10.1021/acs.iecr.9b03048.
24 S. D. Schaber, D. I. Gerogiorgis, R. Ramachandran, J. M. B. Evans, P. I. Barton and B. L. Trout, Economic Analysis of Integrated Continuous and Batch Pharmaceutical Manufacturing: A Case Study, *Ind. Eng. Chem. Res.*, 2011, **50**, 10083–10092, DOI: 10.1021/ie2006752.
25 ICH, *Q13 Continuous Manufacturing of Drug Substances and Drug Products*, 2021.
26 A. Adamo, R. Beingessner, M. Behnam, J. Chen, T. Jamison, K. Jensen, J.-C. Monbaliu, A. Myerson, E. Revalor, D. Snead, T. Stelzer, N. Weeranoppanant, S. Y. Wong and P. Zhang, On-Demand Continuous-Flow Production of Pharmaceuticals in a Compact, Reconfigurable System, *Science*, 2016, **352**, 61–67, DOI: 10.1126/science.aaf1337.
27 P. Zhang, N. Weeranoppanant, D. A. Thomas, K. Tahara, T. Stelzer, M. G. Russell, M. O'Mahony, A. S. Myerson, H. Lin, L. P. Kelly, K. F. Jensen, T. F. Jamison, C. Dai, Y. Cui, N. Briggs, R. L. Beingessner and A. Adamo, Advanced Continuous Flow Platform for On-Demand Pharmaceutical Manufacturing, *Chem. – Eur. J.*, 2018, **24**, 2776–2784, DOI: 10.1002/chem.201706004.
28 P. L. Heider, S. C. Born, S. Basak, B. Benyahia, R. Lakerveld, H. Zhang, R. Hogan, L. Buchbinder, A. Wolfe, S. Mascia, J. M. B. Evans, T. F. Jamison and K. F. Jensen, Development of a Multi-Step Synthesis and Workup Sequence for an Integrated, Continuous Manufacturing Process of a Pharmaceutical, *Org. Process Res. Dev.*, 2014, **18**, 402–409, DOI: 10.1021/op400294z.
29 S. Mascia, P. L. Heider, H. Zhang, R. Lakerveld, B. Benyahia, P. I. Barton, R. D. Braatz, C. L. Cooney, J. M. B. Evans, T. F. Jamison, K. F. Jensen, A. S. Myerson and B. L. Trout, End-to-End Continuous Manufacturing of Pharmaceuticals: Integrated Synthesis, Purification, and Final Dosage Formation, *Angew. Chem., Int. Ed.*, 2013, **52**, 12359–12363, DOI: 10.1002/anie.201305429.
30 R. Lakerveld, P. L. Heider, K. D. Jensen, R. D. Braatz, K. F. Jensen, A. S. Myerson and B. L. Trout, End to End Continuous: Integration of Unit Operations, in *Continuous Manufacturing of Pharmaceuticals*, ed. P. Kleinebudde, J. Khinast and J. Rantanen, John Wiley & Sons Ltd, 2017, pp. 447–483.
31 FDA, *FDA Drug Shortages Current and Resolved Drug Shortages and Discontinuations Reported to FDA*, https://www.accessdata.fda.gov/scripts/drugshortages/dsp_ActiveIngredientDetails.cfm.
32 D. Hartley, D. Jack, L. Lunts and A. Ritchie, New Class of Selective Stimulants of Beta-Adrenergic Receptors, *Nature*, 1968, **219**, 861–862, DOI: 10.1038/219861a0.
33 L. Marques and N. Vale, Salbutamol in the Management of Asthma: A Review, *Int. J. Mol. Sci.*, 2022, **23**, 14207, DOI: 10.3390/ijms232214207.
34 FDA, Drug Shortages, 2022.
35 U.S. Food and Drug Administration, FDA Drug Shortages, https://www.accessdata.fda.gov/scripts/drugshortages/dsp_ActiveIngredientDetails.cfm, (accessed 18 December 2025).

36 A. A. Kazi, B. V. Subba Reddy and L. Ravithej Singh, Synthetic Approaches to FDA Approved Drugs for Asthma and COPD from 1969 to 2020, *Bioorg. Med. Chem.*, 2021, **41**, 116212, DOI: 10.1016/j.bmc.2021.116212.
37 R. Vardanyan and V. Hruby, in *Synthesis of Best-Seller Drugs*, Elsevier, 2016, pp. 189–199.
38 S. Y. Skachilova, E. F. Zueva, I. D. Muravskaya, L. V. Goncharenko and L. D. Smirnov, Methods for the Preparation of Salbutamol, *Methods Synth. Technol. Prod. Drugs*, 1992, 733–739.
39 D. Collin, D. Hartley, D. Jack, L. Lunts, J. Press, A. Ritchie and P. Toon, Analogs of Sympathomimetic Catecholamines, *J. Med. Chem.*, 1970, **13**, 674–680.
40 L. H. Lunts and P. Toon, Phenylaminoethanol Derivatives, *US Pat.*, 3705233, 1972.
41 H. Lunts and P. Toon, 4, Hydroxy-Alpha' Aminomethyl-m-Xylene-Alpha', Alpha-3-Diols, *US Pat.*, 3644353, 1972.
42 E. Babad, N. I. Carruthers, R. S. Jaret and M. Steinman, A Short Synthesis of Albuterol, *Synthesis*, 1988, 966–968, DOI: 10.1055/s-1988-27768.
43 C. Tann, T. Thiruvengadam, J. Chiu, M. Green, T. McAllister, C. Colon and J. Lee, Process for Preparing Albuterol, Acetal, Hemi-Acetal, and Hydrates of Arylglyoxal Intermediates Thereof, WO9204314, 1992.
44 W. G. Lee, M. T. Zell, T. Ouchi and M. J. Milton, NMR Spectroscopy Goes Mobile: Using NMR as Process Analytical Technology at the Fume Hood, *Magn. Reson. Chem.*, 2020, **58**, 1193–1202, DOI: 10.1002/mrc.5035.
45 F. Carey and R. Sundberg, in *Advanced Organic Chemistry Part A: Structure and Mechanisms*, Kluwer Academic/Plenum Publishers, Boston, 4th edn, 2000, pp. 267–269.
46 O. Levenspiel, Chemical Reaction Engineering, *Ind. Eng. Chem. Res.*, 1999, **38**, 4140–4143, DOI: 10.1021/ie990488g.
47 S. Fogler, *Elements of Chemical Reaction Engineering*, Pearson Education Ltd., 6th edn, 2022.
48 D. Hartley and D. Middlemiss, Absolute Configuration of the Optical Isomers of Salbutamol, *J. Med. Chem.*, 1971, **14**, 895–896, DOI: 10.1021/jm00291a036.
49 D. G. Gregory, K. E. Kay, J. T. Turnage, K. E. Penzer and J. K. Ferri, Development of an Advanced Manufacturing Technology for Continuous Drug Substance Production, *Ind. Eng. Chem. Res.*, 2026, DOI: 10.1021/acs.iecr.5c04185.
50 T. Schikarski, H. Trzenschiok, W. Peukert and M. Avila, Inflow Boundary Conditions Determine T-Mixer Efficiency, *React. Chem. Eng.*, 2019, **4**, 559–568, DOI: 10.1039/c8re00208h.
51 R. J. T. Kleijwegt, V. C. Henricks, W. Winkenwerder, W. Baan and J. Van Der Schaaf, Renewable Dimethyl Carbonate for Tertiary Amine Quaternisation: Kinetic Measurements and Process Optimisation, *React. Chem. Eng.*, 2021, **6**, 2125–2139, DOI: 10.1039/d1re00191d.
52 C. J. Taylor, J. A. Manson, G. Clemens, B. A. Taylor, T. W. Chamberlain and R. A. Bourne, Modern Advancements in Continuous-Flow Aided Kinetic Analysis, *React. Chem. Eng.*, 2022, **7**, 1037–1046, DOI: 10.1039/d1re00467k.
53 K. T. Nguyen and D. V. Papavassiliou, Flow Effects on the Kinetics of a Second-Order Reaction, *Chem. Eng. J.*, 2008, **140**, 370–380, DOI: 10.1016/j.cej.2007.10.021.
54 T. A. Hamlin, M. Swart and F. M. Bickelhaupt, Nucleophilic Substitution (SN2): Dependence on Nucleophile, Leaving Group, Central Atom, Substituents, and Solvent, *ChemPhysChem*, 2018, **19**, 1315–1330, DOI: 10.1002/cphc.201701363.
55 F. Carey and R. Sundberg, in *Advanced Organic Chemistry Part B: Reactions and Synthesis*, Kluwer Academic/Plenum Publishers, Boston, 4th edn, 2000, pp. 155–157.
56 W. Morris, E. D. Lorance and I. R. Gould, Understanding the Solvent Contribution to Chemical Reaction Barriers, *J. Phys. Chem. A*, 2019, **123**, 10490–10499, DOI: 10.1021/acs.jpca.9b06310.
57 K. Burger, *Studies in Analytical Chemistry*, 1983, vol. 6, pp. 203–216.
58 Y. Ben-Tal, P. J. Boaler, H. J. A. Dale, R. E. Dooley, N. A. Fohn, Y. Gao, A. García-Domínguez, K. M. Grant, A. M. R. Hall, H. L. D. Hayes, M. M. Kucharski, R. Wei and G. C. Lloyd-Jones, Mechanistic Analysis by NMR Spectroscopy: A Users Guide, *Prog. Nucl. Magn. Reson. Spectrosc.*, 2022, **129**, 28–106, DOI: 10.1016/j.pnmrs.2022.01.001.
59 Z. J. Tian, Y. Dai, F. Hu, Z. H. Shen, H. L. Xu, H. W. Zhang, J. H. Xu, Y. T. Hu, Y. Y. Diao and H. L. Li, Enhancing Chemical Reaction Monitoring with a Deep Learning Model for NMR Spectra Image Matching to Target Compounds, *J. Chem. Inf. Model.*, 2024, **64**, 5624–5633, DOI: 10.1021/acs.jcim.4c00522.
60 ICH, *Guideline for Elemental Impurities Q3D(R1)*, 2019.
61 J. Turnage, D. Gregory and J. Ferri, Tangential Flow Filtration Enables Continuous API Manufacturing: Case Study of Albuterol Sulfate, *Chem. Eng. Sci.*, 2026, **320**, 122500, DOI: 10.1016/j.ces.2025.122500.